consist of similar amounts of V^{4+} (24 and 29%), with the remainder being V^{5+}. Samples derived from the VPO hemihydrate that were heated in N_2 to temperatures in the range from 550° to 750°C and cooled in N_2 contained no surface V^{5+} species.

Because the sample of ω-$VOPO_4$ that was cooled to room temperature was found to have surface V^{4+}, we investigated the transformation of ω-$VOPO_4$ using in situ EPR spectroscopy (Fig. 4B). The ω-$VOPO_4$ was reformed in the EPR cell at 400°C in the presence of air. *n*-Butane was then added to the cell/catalyst, and the spectra were collected continuously. The results showed an immediate, albeit small, change in the X-band EPR spectrum (Fig. 4B) after exposure to *n*-butane. This change occurred within the first 5 min after *n*-butane addition. After 90 min, no further change occurred in the spectra. This result supports the fast transformation observed in the XRD experiments. Because of the poor resolution of the high-temperature EPR spectra, the room-temperature spectra of ω-$VOPO_4$ and δ-$VOPO_4$ were also recorded at higher Q-band frequencies, in order to obtain more accurate spin Hamiltonian parameters (fig. S10). Analysis of these parameters revealed slight differences in the crystal field parameters α and Δ (*17*), indicating an increased extent of tetragonal distortion in the VO_6 units for the δ-$VOPO_4$ sample, as would be expected from the removal of lattice oxygen. Furthermore, an increased V^{4+} signal intensity was observed for δ-$VOPO_4$ as compared to ω-$VOPO_4$ (from 1.0 to 1.2 arbitrary units), which is in agreement with the XPS observation (24 to 29%, respectively).

Based on these complementary in situ experiments, we conclude that the phase transition from ω-$VOPO_4$ to δ-$VOPO_4$ appears to be directly connected with the oxidizing action of the catalyst and its reactivity toward the gas-phase components. For example, *n*-butane and acetic acid rapidly induce a phase change, and it is known that VPOs are very reactive toward these materials. The effect is less pronounced with CO and H_2, which are less potent reducing agents for VPOs, and maleic anhydride does not display any effect.

We propose that the transition from ω-$VOPO_4$ to δ-$VOPO_4$ is only possible with a certain minimum concentration of surface oxygen vacancies, in order to facilitate the oxygen mobility necessary to rearrange the structure. Overall, this transition is clearly a reduction process, but it has to be considered as too small a degree of reduction to be a bulk process; otherwise, ω-$VOPO_4$ and δ-$VOPO_4$ could not be considered as polymorphs because there would have to be a change in stoichiometry. The experimental evidence (that in the absence of air, δ-$VOPO_4$ evolves to a disordered material in which it is possible to regenerate to ω-$VOPO_4$ only if air is used) can be explained by the formation of a large number of oxygen vacancies involving bulk reduction (scheme S1). δ-$VOPO_4$ can be recrystallized to ω-$VOPO_4$ when the sample is heated at 600°C in air, and the formation of δ-$VOPO_4$ from ω-$VOPO_4$ occurs only with a suitable reducing agent at 400°C; although at 600°C, no reaction occurs in the absence of O_2. These are indications of the metastability of the ω-$VOPO_4$ phase, with ω-$VOPO_4$ being more stable than δ-$VOPO_4$ at high temperatures, whereas the opposite is true at 400°C. The disordered material can also be fully recrystallized to ω-$VOPO_4$ when the oxygen is replaced at 600°C.

The observation that the Raman spectrum of ω-$VOPO_4$ is very similar to that of δ-$VOPO_4$ is relevant to previous in situ spectroscopic studies of VPO catalysts. In previous studies, the assignment of the presence of δ-$VOPO_4$ was often based on Raman spectroscopy. Thus, the formation of ω-$VOPO_4$ during the industrial process can be considered possible, particularly during the formation of the calcined catalyst precursor. Obviously, ω-$VOPO_4$ cannot be involved in the main catalytic process because we observed its rapid transformation to δ-$VOPO_4$ in the presence of the reactants, but the ω-$VOPO_4$ phase could play an important role in the activation of the catalyst. For example, ω-$VOPO_4$ could be involved in the formation of a certain amount of V^{5+} (*7*, *8*), which is recognized to be important for improving the catalyst performance (*10*).

References and Notes

1. P. Amorós, D. Marcos, A. Beltrán-Porter, D. Beltrán-Porter, *Curr. Opin. Solid State Mater. Sci.* **4**, 123 (1999).
2. G. Villeneuve, K. S. Suh, P. Amorós, N. Casañ-Pastor, D. Beltrán, *Chem. Mater.* **4**, 108 (1992).
3. G. Centi, Ed., vol. 16 of *Catalysis Today* (Elsevier, Amsterdam, 1993), part 1.
4. E. Bordes, *Catal. Today* **1**, 499 (1987).
5. G. J. Hutchings *et al.*, *J. Catal.* **208**, 197 (2002).
6. G. J. Hutchings, *J. Mater. Chem.* **14**, 3385 (2004).
7. G. J. Hutchings, A. Desmartin Chomel, R. Olier, J. C. Volta, *Nature* **368**, 41 (1994).
8. G. W. Coulston *et al.*, *Science* **275**, 191 (1997).
9. H. Wibbeke, International Centre for Diffraction Data, Powder Diffraction File, Entry 37-809 (1996).
10. P. Amorós *et al.*, *J. Phys. Chem. Solids* **62**, 1393 (2001).
11. G. J. Hutchings, *Appl. Catal.* **72**, 1 (1991).
12. M. Dente, S. Pierucci, E. Tronconi, M. Cecchini, F. Ghelfi, *Chem. Eng. Sci.* **58**, 643 (2003).
13. J. C. Burnett, R. A. Keppel, W. D. Robinson, *Catal. Today* **1**, 537 (1987).
14. R. M. Contractor, *Chem. Eng. Sci.* **54**, 5627 (1999).
15. J. T. Gleaves, J. R. Ebner, T. C. Kuechler, *Catal. Rev. Sci. Eng.* **30**, 49 (1988).
16. Precursors prepared by different routes behaved identically in the experiments described in this paper. Therefore, we do not consider that our findings relate to a specific preparation of $VOHPO_4{\cdot}0.5H_2O$ or to a specific morphology, but we believe that our results have general applicability.
17. Additional data are available on *Science* Online.
18. F. Girgsdies *et al.*, poster presented at the XXXIX Jahrestreffen Deutscher Katalytiker meeting, Weimar, Germany, 15 to 17 March 2006 (http://edoc.mpg.de/display.epl?mode=doc&id=263374 and in the supporting online material).
19. T. Ressler *et al.*, *J. Catal.* **191**, 75 (2000).

20. We thank the Engineering and Physical Sciences Research Council for financial support.

Supporting Online Material

www.sciencemag.org/cgi/content/full/313/5791/1270/DC1
Materials and Methods
Figs. S1 to S10
Table S1
References
Scheme S1
Poster S1

25 May 2006; accepted 19 July 2006
10.1126/science.1130493

Fluorous Nanodroplets Structurally Confined in an Organopalladium Sphere

Sota Sato,[1] Junya Iida,[1] Kosuke Suzuki,[1] Masaki Kawano,[1] Tomoji Ozeki,[2] Makoto Fujita[1]*

The distinct properties of fluorous phases are practically useful for separation, purification, and reaction control in organic synthesis. Here, we report the formation of a liquid-like fluorous droplet, composed of 24 perfluoroalkyl chains confined in the interior of a 5-nanometer-sized, roughly spherical shell that spontaneously assembled in solution from 12 palladium ions and 24 bridging ligands. Crystallographic analysis confirmed the rigid shell framework and amorphous interior. Perfluoroalkanes can dissolve in this well-defined fluorous phase, whereas they can hardly dissolve in a surrounding polar organic solution, and their solubility (up to ~eight perfluoroalkane molecules per spherical complex) can be finely controlled by tuning the length of perfluoroalkyl chains tethered to the shell.

A fluorous phase manifests distinct solubilizing properties relative to aqueous and common organic phases and therefore proves useful for a range of separation (*1*–*3*), purification (*4*, *5*), and catalyst-immobilization (*6*–*8*) techniques. In particular, organic synthesis using the fluorous phase has developed rapidly in recent years (*9*) because of its high compatibility with environmentally benign chemistry. Nanometer-scale fluorous environments can be attained within vesicles, micelles, or dendrimers that in turn dissolve in aqueous or organic solvents; however, the phases are often poorly defined physically and structurally (*10*–*12*). We previously showed (*13*, *14*) that pyridine-capped banana-shaped bridging ligands spontaneously

assembled in solution with metal ions to form ~5-nm-diameter spherical shells. Here, we report that, by attaching a perfluoroalkyl group at the curvature point of the ligand, we obtained an $M_{12}L_{24}$ (where M represents a metal and L a ligand) spherical complex whose interior is filled with 24 perfluoroalkyl chains (Fig. 1). The interior of the complex can be regarded as a structurally well-confined, molecular-scale fluorous "droplet" (Fig. 1) that can selectively dissolve fluorocarbons, whereas a surrounding solution can hardly dissolve them.

Ligands **1a** to **1d** (Fig. 1) were prepared in high yield from the Mitsunobu or the Williamson reaction of the corresponding $R_FCH_2CH_2OH$ or $R_FCH_2CH_2I$ precursor, respectively, with 2,6-dibromophenol, followed by Sonogashira cross-coupling with 4-ethynylpyridine. When a mixture of ligand **1a** (11 μmol) and $Pd(NO_3)_2$ (9.1 μmol) in dimethyl sulfoxide (DMSO)–d_6 (0.70 ml) was heated at 70°C for 3 hours, the endofluorous $M_{12}L_{24}$ complex **2a** was quantitatively obtained, as indicated by nuclear magnetic resonance (NMR) spectroscopy (vide infra). Complexes **2b** to **2d** were quantitatively prepared by the same method.

After counterion exchange with triflate ion (OTf^-), the $M_{12}L_{24}$ stoichiometry of **2a** was confirmed by cold-spray ionization mass spectrometry (CSI-MS) (Fig. 2): From a series of prominent peaks of $[\mathbf{2a}\text{-}(OTf^-)_m + (DMSO)_n]^{m+}$ (with m values from 8 to 14 and n values of 0 or 1), the molecular weight was determined to be 20,276.5 (calculated as 20,272.2). In ^1H and ^{19}F NMR spectra, only one set of signals was observed for the ligand **1a** nuclei, consistent with the cuboctahedron symmetry of **2a** (Fig. 2). The observed large downfield shift of pyridine (Py) H_α and PyH_β protons [Δδ equal to 0.59 and 0.23 parts per million (ppm), respectively] is characteristic of pyridine-metal coordination. In ^{19}F NMR, signals for the C_6F_{13} chain were unambiguously assigned by ^{19}F-^{19}F nuclear Overhauser effect spectroscopy (NOESY) and correlation spectroscopy (COSY) experiments (*15*). In a similar manner, endofluorinated $M_{12}L_{24}$ spheres **2b** to **2d** were fully characterized. The diffusion coefficient of **2a** to **2d**, determined by diffusion-ordered NMR spectroscopy (DOSY) experiments using both ^1H and ^{19}F nuclei, was $D = 4.0 \times 10^{-11} \pm 0.5 \times 10^{-11}$ m^2 s^{-1}, consistent with the estimated diameter of 4.3 nm (*13*, *14*). We also obtained clear atomic force microscopy (AFM) images for **2a** to **2d** that indicated diameters of 4.9 ± 0.3 nm (fig. S8).

We expected that the fluorous core of **2a** could accommodate (or dissolve) fluorinated compounds through fluorophilic host-guest interaction. Thus, excess perfluorooctane, **3**, which is hardly soluble in DMSO, was suspended in a DMSO-d_6 solution of **2a** (0.43 mM), and the mixture was stirred vigorously at room temperature for 2 hours. Unencapsulated **3** was then separated by phase separation in a centrifuge, and the DMSO-d_6 solution was analyzed by ^{19}F NMR (Fig. 3). In addition to the signals from the C_6F_{13} chains of **2a**, we observed a set of four signals for included guests **3**. From the integral ratio, it was estimated that on average 5.8 molecules of **3** were accommodated by **2a**. This host-guest ratio remained almost unchanged even when the experiment was carried out at different concentrations (**2a** concentrations of 0.18, 0.37, or 0.54 mM). Detailed analysis of ^{19}F NMR spectra showed that the signals of the terminal fluorine atoms in the C_6F_{13} chain of **2a** were shifted further upfield than internal ones: Δδ ranged from 0.4 to 1.3 ppm for F^{d-f} and from 0.0 to 0.1 ppm for F^{a-c} (Fig. 3). On the basis of this finding, we assume that guest molecules accumulate at the core of the hollow complex. The guest signals are also shifted upfield relative to the signals of free perfluorooctane in $CDCl_3$ (Δδ from 1.3 to 2.3 ppm). The guest, **3**, can be drawn out from the interior of **2a** by addition of acetonitrile to the solution, because **3** can dissolve in the mixed solvent (Materials and Methods).

DOSY experiments afforded further evidence for the inclusion of **3** in **2a**. In ^{19}F DOSY NMR spectra, a single band consisting of signals from both **2a** and **3** was observed at $D = 3.2 \times 10^{-11}$ m^2 s^{-1} (Fig. 3B). Because the diffusion coefficient of free perfluorooctane is much larger ($D = 1.3 \times 10^{-9}$ m^2 s^{-1} in $CDCl_3$), the observed coincidence of diffusion coefficients indicates the association of **2a** with **3**.

Crystallography revealed that the complex, **2a**, possesses a raw egg–like structure, in which a rigid $M_{12}L_{24}$ shell framework encloses flexible, disordered perfluoroalkyl chains that resemble a liquid (Fig. 4). Single crystals of the **2a**•(**3**)$_n$ complex were obtained by slow vapor diffusion of ethyl acetate into a DMSO solution of **2a**•(**3**)$_n$ (n = 5.8). Although a conventional laboratory diffractometer afforded data with insufficient resolution to determine the structure, the use of synchrotron x-ray radiation provided impressive-

[1]Department of Applied Chemistry, School of Engineering, University of Tokyo, and Core Research for Evolutional Science and Technology (CREST), Japan Science and Technology Corporation (JST), 7-3-1 Hongo, Bunkyo-ku, Tokyo 113-8656, Japan. [2]Department of Chemistry and Materials Science, Tokyo Institute of Technology, 2-12-1 O-okayama, Meguro-ku, Tokyo 152-8551, Japan.

*To whom correspondence should be addressed. E-mail: mfujita@appchem.t.u-tokyo.ac.jp

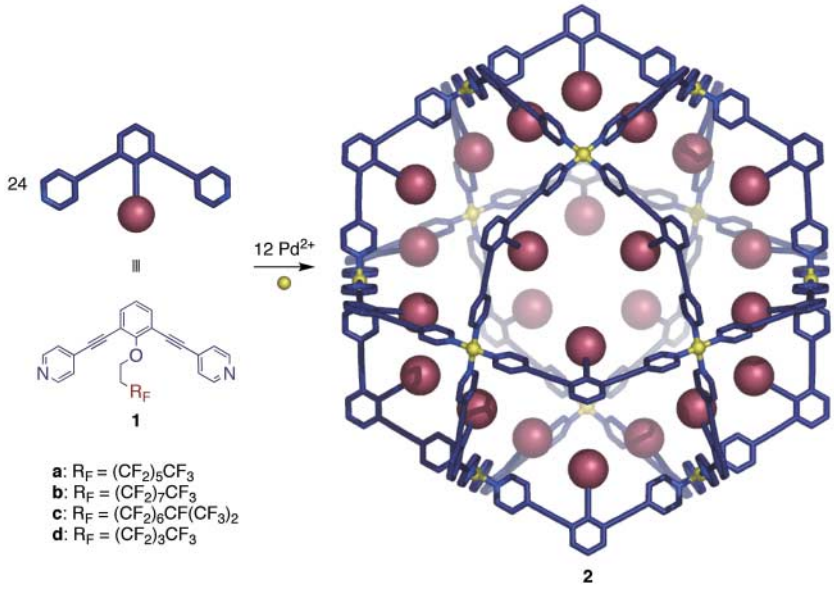

Fig. 1. Self-assembly of endofluorous $M_{12}L_{24}$ molecular spheres.

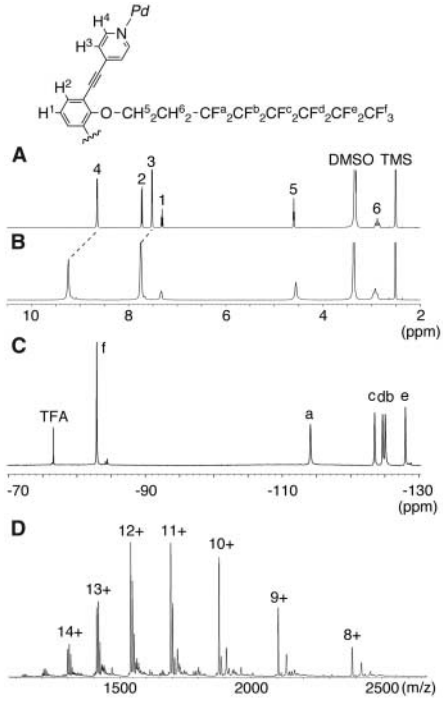

Fig. 2. (**A**) ^1H NMR spectrum of **1a**. (**B**) ^1H and (**C**) ^{19}F NMR spectra of **2a**. (**D**) CSI-MS spectrum of **2a** (CH_3CN:DMSO = 19:1, OTf^- salt).

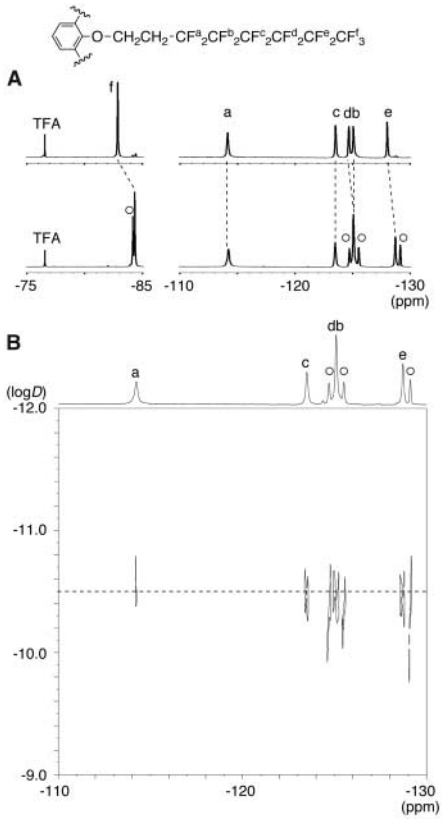

Fig. 3. (**A**) ^{19}F NMR spectra (470 MHz, DMSO-d_6) of (top) complex **2a** and (bottom) inclusion complex of **2a** and **3** (indicated in circles). (**B**) DOSY spectrum of inclusion complex of **2a** and **3**.

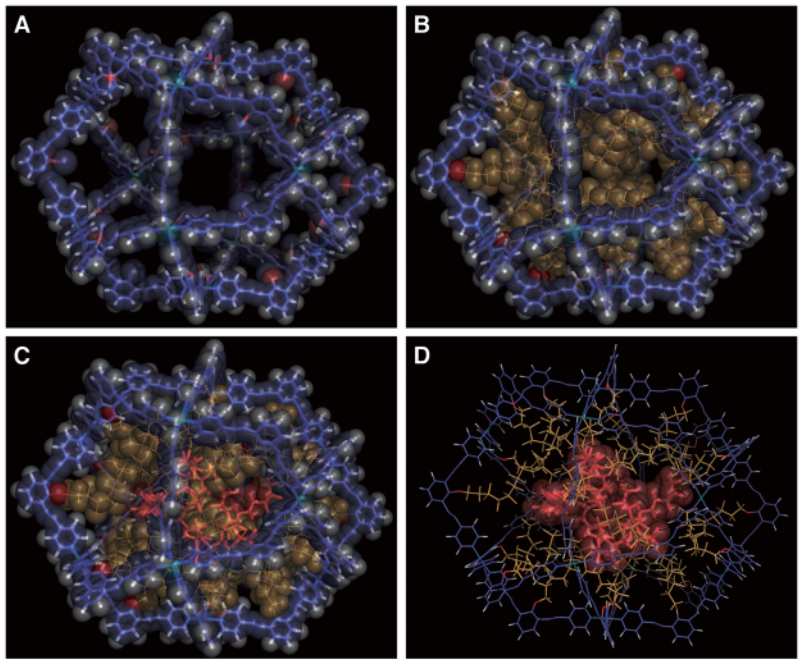

Fig. 4. Molecular structure of **2a**. (**A**) The *x*-ray crystal structure of the shell framework of **2a**. $C_6F_{13}CH_2$- side chains at the curvature point of the ligands are disordered and could not be located. (**B**) The $C_6F_{13}(CH_2)_2$- side chains (orange) are modeled, and only the chains are optimized, by force-field calculations. (**C** and **D**) Six molecules of perfluorooctane (**3**, red) were placed at the central void of **2a**, and structural annealing was conducted from 2000 to 300 K by molecular dynamics (MD) simulation. The images show one of the energy minimum structures obtained after MD simulation followed by force-field optimization. In (D), host **2a** is represented by wire frames, whereas the accommodated guest molecules are represented by space-filling models.

ly higher quality data, from which the $M_{12}L_{24}$ shell framework of **2a** could be refined (*16*). The fluorous chains and the included guest, **3**, are completely disordered and cannot be located in the crystallographic analysis. The shell framework is shown to be not spherical but oval, with a dimension of 4.9 nm by 4.2 nm (Fig. 4A). The distortion from the ideal spherical shape is probably induced by the aggregation of the fluorous chains in the shell.

To elucidate how the host, **2a**, accommodates the guest, **3**, we carried out force-field calculations: 24 $C_6F_{13}(CH_2)_2$- side chains were attached to the residual oxygen atoms of the ligand **1a** components in the crystal structure of **2a**, and only the side chains were optimized. The optimized structure shows that, despite the aggregation of the fluorous chains, a void remains at the core (Fig. 4B). Therefore, we added six perfluorooctane molecules to the void and minimized the whole structure by molecular dynamics simulation. Repeated, gradual annealing from 2000 to 300 K accumulated energy-minimized structures 30 times. All of these minimized structures converged almost identically to a structure in which the guest molecules interact with the terminal $CF_3CF_2CF_2$- portions of the perfluoroalkyl side chains (Fig. 4, C and D). This arrangement is consistent with the NMR spectra that show large upfield shifts of the signals from the terminal $CF_3CF_2CF_2$- groups. We emphasize that the guest molecules **3** are dissolved, rather than recognized, in a well-defined fluorous droplet composed of 24 C_6F_{13} side chains.

Because of the well-defined, precise structure of the $M_{12}L_{24}$ framework, the fluorous environment and the void space at the core are predictable and easily controlled by modifying the fluorinated side chain of the ligand. Sphere **2b** with $(CF_2)_7CF_3$ groups, or sphere **2c** with more bulky $(CF_2)_6CF(CF_3)_2$ groups, accommodated a smaller amount of perfluorooctane (circa 2.5 guest molecules per complexes), presumably due to reduced effective void volume at the core of the sphere. In contrast, sphere **2d**, with sterically less-demanding $(CF_2)_3CF_3$ side chains, evidenced no inclusion of perfluorooctane despite a larger void space in the sphere, perhaps because of insufficient fluorine density to define the fluorous atmosphere. Sphere **2a** included other fluorocarbons such as perfluorohexane (~8.0 molecules per **2a**) but not fluoroaromatics such as perfluorobenzene or perfluoronaphthalene, presumably because of better interaction with the external solvent. Further ligand tuning should enhance the viability of these fluorous droplets for mediating reaction chemistry.

References and Notes

1. A. Studer *et al.*, *Science* **275**, 823 (1997).
2. J. Yoshida, K. Itami, *Chem. Rev.* **102**, 3693 (2002).
3. J. A. Gladysz, D. P. Curran, I. T. Horváth, Eds., *Handbook of Fluorous Chemistry* (Wiley-VCH, Weinheim, Germany, 2004), chaps. 4 and 7.
4. A. Studer, P. Jeger, P. Wipf, D. P. Curran, *J. Org. Chem.* **62**, 2917 (1997).
5. W. Zhang, *Tetrahedron* **59**, 4475 (2003).
6. I. T. Horváth, J. Rábai, *Science* **266**, 72 (1994).
7. I. T. Horváth, *Acc. Chem. Rev.* **31**, 641 (1998).
8. R. H. Fish, *Chem. Eur. J.* **5**, 1677 (1999).
9. P. Kirsch, *Modern Fluoroorganic Chemistry* (Wiley-VCH, Weinheim, Germany, 2004), chap. 3.
10. M. P. Krafft, *Adv. Drug Delivery Rev.* **47**, 209 (2001).
11. J. G. Riess, *Tetrahedron* **58**, 4113 (2002).
12. K. C. Hoang, S. Mecozzi, *Langmuir* **20**, 7347 (2004).
13. M. Tominaga *et al.*, *Angew. Chem. Int. Ed. Engl.* **43**, 5621 (2004).
14. M. Tominaga, K. Suzuki, T. Murase, M. Fujita, *J. Am. Chem. Soc.* **127**, 11950 (2005).
15. J. L. Battiste, N. Jing, R. A. Newmark, *J. Fluorine Chem.* **125**, 1331 (2004).
16. X-ray crystallographic analysis of **2a**: The diffraction data were measured at 130 K [wavelength (λ) = 0.6890 Å] at Photon Factory–Advanced Ring for Pulse X-rays (PF-AR) of the High Energy Accelerator Research Organization (KEK). Space group *I*4/*m*, temperature (T) = 130 ± 2, a = 43.970 ± 0.006 Å, b = 43.970 ± 0.006 Å, c = 42.521 ± 0.009 Å, volume (V) = 82,208 ± 23 Å^3, atomic number (Z) = 1. Anisotropic least-squares refinement for the palladium atoms and isotropic refinement for the other atoms on 8023 independent merged reflections (R_{int} = 0.1329) converged at residual $wR_2(F^2)$ = 0.3243 for all data; residual $R_1(F)$ equals 0.2460 for 3472 observed data [$I > 2\sigma(I)$], and goodness of fit (GOF) equals 1.965. The successful refinement of the shell framework is remarkable because the framework crystallographically determined occupies only 13% of the extraordinary large cell volume (82,208 Å^3). The remaining volume of 87% is occupied by severely disordered

perfluoroalkyl chains, guest **5**, solvents, and counter ions. Hence the *R* value of 24.6% is quite reasonable given the size and complexity of the compound.
17. This work was financially supported by a Grant-in-Aid for Scientific Research (S) no. 14103014, from the Ministry of Education, Culture, Sports, Science, and Technology of Japan. Supplementary crystallographic data for compound **2a** can be obtained free of charge (under CCDC 602076) by contacting the Cambridge Crystallographic Data Centre, 12, Union Road, Cambridge CB2 1EZ, UK; via their Web site (www.ccdc.cam.ac.uk/data_request/cif), by e-mail (data_request@ccdc.cam.ac.uk), or by fax (+44 1223 336033). We thank K. Yamaguchi and H. Masu for CHNS elemental analyses.

Supporting Online Material
www.sciencemag.org/cgi/content/full/313/5791/1273/DC1
Materials and Methods
Figs. S1 to S8

11 May 2006; accepted 20 July 2006
10.1126/science.1129830

Triple-Bond Reactivity of Diphosphorus Molecules

Nicholas A. Piro, Joshua S. Figueroa, Jessica T. McKellar, Christopher C. Cummins*

We report a mild method for generating the diphosphorus molecule or its synthetic equivalent in homogeneous solution; the P_2 allotrope of the element phosphorus is normally obtained only under extreme conditions (for example, from P_4 at 1100 kelvin). Diphosphorus is extruded from a niobium complex designed for this purpose and can be trapped efficiently by two equivalents of an organic diene to produce an organodiphosphorus compound. Diphosphorus stabilized by coordination to tungsten pentacarbonyl can be generated similarly at 25°C, and in this stabilized form it still efficiently consumes two organic diene molecules for every diphosphorus unit.

A dichotomy exists in the chemistry of the group 15 elements: The stable molecular form of nitrogen is triply bonded dinitrogen, whereas the stable molecular form of phosphorus is the tetrahedral P_4 molecule, white phosphorus (*1*). Only upon heating white phosphorus to more than 1100 K does the P_4 = 2 P_2 equilibrium become important (*2*–*4*). Underlying this dichotomy is the tendency of nitrogen to engage in multiple bonding, as compared with phosphorus, for which the π-bond components of multiple bonds are relatively high in energy and quite reactive (*5*, *6*). Thus, the triple bond in the atmospherically abundant dinitrogen molecule is one of the strongest known chemical bonds (its bond dissociation enthalpy, D_e, is 226 kcal/mol), whereas that in the diphosphorus molecule is only about half as strong (D_e = 117 kcal/mol) (*7*, *8*). P_2 is therefore known principally as an exotic gas-phase species of astrophysical interest (*9*), as a reactive component of plasmas generated in the high-temperature deposition of III/V semiconductor materials (*10*), and in the context of matrix-isolation experiments (*11*–*14*). The use of P_2 in chemical synthesis requires a means to generate it in solution and under mild conditions of temperature and pressure. Accordingly, we describe a mild method that uses niobium chemistry as a vehicle for the generation of diphosphorus (or a synthetic equivalent) in solution, where it may be trapped by suitable organic acceptors.

Organic azides, molecules of formula N=N=N–R, where R is a variable organic substituent, are known to react with transfer of their nitrene moiety (N–R) to a group 5 metal through observable or isolable intermediates, in which an intact RN_3 molecule is complexed (*15*–*17*). The final products in such a nitrene transfer reaction are the group 5 metal imido and N_2 gas (Fig. 1A). Diphosphorus-substituted analogs of organic azides, of formula P=P=N–R, would be a useful addition to the library of low-coordinate phosphorus compounds (*5*), and we wondered whether they would react analogously with group 5 metals to transfer nitrene while extruding the desired P_2 molecule (Fig. 1B).

To synthesize such a solution-phase P_2-generating molecular system, we created the phosphorus-phosphorus bond within the protective coordination sphere of a niobium complex. Recently, we have used the terminal phosphide anion $[P{\equiv}Nb(N[Np]Ar)_3]^{1-}$ (where Np is neopentyl and Ar is 3,5-$C_6H_3Me_2$) as its sodium salt to great advantage in assembling phosphorus-element bonds atop the protective $Nb(N[Np]Ar)_3$ platform (*18*, *19*), and the present work is a logical extension of that methodology.

The system (η^2-Mes*NPP)$Nb(N[Np]Ar)_3$ (where Mes* is 2,4,6-*t*-$Bu_3C_6H_2$), **1**, containing the diphosphorus-substituted organic azide ligand bound through its P_2 unit to the niobium trisanilide platform, has been obtained in 60% isolated yield as an orange-red solid after an NaCl-elimination reaction between Niecke's chloroiminophosphane ClP=NMes* (*20*) and our terminal phosphide anion sodium salt, $Na[P{\equiv}Nb(N[Np]Ar)_3]$ (*21*). Complex **1** has been characterized by single-crystal x-ray crystallography (Fig. 2A); the structure so obtained is notable for its short P=P and P=N interatomic distances [2.0171(±0.0009) and 1.556 (±0.002) Å (where the error is estimated standard deviation), respectively], which suggest multiple bonding between these atoms. Characterization data for **1** obtained by nuclear magnetic resonance (NMR) spectroscopy (^{31}P, ^{13}C, and ^{1}H) in benzene-d_6 solution are consistent with the observed solid-state structure of the complex, with the ^{31}P data [doublets with a one-bond P-P coupling constant $^{1}J_{PP}$ = 650 Hz at a chemical shift, δ, of 334 and 315 parts per million (ppm)] being most diagnostic for the system. Alternative isomeric formulations of **1** may be similar in energy to the solid-state structure of **1**, and we considered them in our computational studies.

Heating a solution of complex **1** in neat 1,3-cyclohexadiene (1,3-CHD), the latter serving both as solvent and as trap for the P_2 unit, to 65°C for 3 hours gave smooth and quantitative conversion to niobium imido **2** together with a single phosphorus-containing product. This product (**3** in Fig. 2A) is characterized by a singlet in the ^{31}P NMR spectrum at δ = −80 ppm. Formulation of **3** as the double Diels-Alder (*22*) adduct of P_2 with two equivalents of 1,3-CHD was confirmed by its isolation in pure form, crystallization, and characterization by single-crystal x-ray crystallography (Fig. 2B). Although P=P double bonds, such as that of the *bis*-$Cr(CO)_5$ complex of diphosphene PhP=PPh (*23*), can react with a diene to form a Diels-Alder adduct, double diene addition to two π bonds of a P_2 unit has not been reported. We propose that this reaction occurs in two steps: (i) transfer of P_2 to the first 1,3-CHD

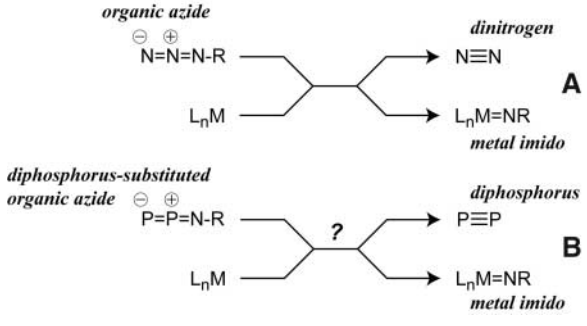

Fig. 1. (**A**) Reaction of an organic azide with a metal complex to extrude dinitrogen while delivering a metal imido unit and (**B**) the envisioned analogous process with diphosphorus extrusion.

Department of Chemistry, Massachusetts Institute of Technology, 77 Massachusetts Avenue, Cambridge, MA 02139–4307, USA.

*To whom correspondence should be addressed. E-mail: ccummins@mit.edu